약학석사학위논문

Tumor microenvironment-modulated reprogramming of tumor cells for the specific delivery of interparticle plasmon nanomaterials

입자간 플라스몬 나노입자의 특이적 전달을 위한 종양미세환경 조절을 이용한 종양세포 재프로그래밍

2019 년 2 월

서울대학교 약학대학원

약학과 물리약학전공

이 다 운

Abstract

Tumor microenvironment-modulated reprogramming of tumor cells for the specific delivery of interparticle plasmon nanomaterials

Da Woon Lee

Physical Pharmacy, Department of Pharmacy

The Graduate School

Seoul National University

Here we report that the modulation of tumor microenvironment can reprogram tumor cells to express specific receptors in greater extent. We prepared the gold and γ-PGA hybrid nanoparticles (Au/PGA hNP) in a facile single step process. In Au/PGA hNP, AuNCs were dispersed in the matrix of the nanoparticles. The pretreatment of the HeLa tumor cells with methylene blue (MB) generated reactive oxygen species (ROS), and reprogrammed the expression levels of gamma glutamyl transferase (GGT) on tumor cell membrane, which is known to

bind to γ-PGA. Consistent with the increased expression of GGT, the delivery of Au/PGA hNP to the tumor cells were significantly enhanced upon the MB pretreatment. Due to the photoresponsiveness of AuNCs and interparticle plasmon coupling between AuNCs inside Au/PGA hNP, the tumor cells taken up higher extents of Au/PGA hNP showed little viability upon irradiation with near infrared (NIR) light. In vivo HeLa-xenografted mice study revealed that the tumor delivery of Au/PGA hNP significantly increased by MB pretreatment. The higher delivery of Au/PGA hNP to the tumor cells resulted in the effective tumor ablation upon NIR illumination. Although we used GGT and Au/PGA hNP to demonstrate the tumor microenvironment ROS-mediated reprogramming, this strategy can be widely applied to overcome the heterogeneity of target receptors by active modulation of tumor microenvironment. Moreover, this strategy can be applicable to the targeted delivery of not only photoresponsive molecules, but also to anticancer chemotherapeutics and other therapeutic cargoes.

Keywords : reprogramming of tumor cells; tumor microenvironment; reactive oxygen species; tumor heterogeneity; receptor-mediated delivery, interparticle plasmon coupling

Student number : 2017-21431

Contents

List of Figures

1. Introduction

Photothermal therapy (PTT) utilizes near-infrared (NIR) light to activate photoresponsive agents and then induce hyperthermia, resulting ablation of tumor of a target site (1). Compared to conventional anticancer therapies, PTT has an advantage of less invasiveness and high selectivity. Organic molecule (2), carbon (3) and metal (4) based nanomaterials have been researched as the photoresponsive agents for PTT. Among them, gold nanoparticles have come into the spotlight as the photothermal agent due to their inertness, capability of absorbing NIR light (5), and high photothermal conversion efficiency due to surface plasmon resonance (SPR) effect (6).

However, gold nanoparticles have some limitations such as their stability in biological fluids (7,8). Chemical conjugation of targeting ligands to gold nanoparticles have been generally used for enhancing specificity of tumor targeting (9,10). But conjugating ligands take additional synthetic steps and cost (11). So using chemical conjugation can be an obstacle to clinical application of gold nanoparticles. Therefore, preparation of gold nanoparticles using a biocompatible matrix without chemical conjugation can maximize their photothermal effects and develop them into practical application.

Poly-γ-glutamic acid (γ-PGA) is a polymer of glutamic acid residues linked by amino bonds between α-amino and γ-carboxyl groups. γ-PGA is biodegradable and

biocompatible (12). γ-PGA coating can reduce nonspecific binding of serum proteins to nanoparticles (13). In addition, γ-PGA is known to bind to gamma-glutamyl transferase (GGT) and then be endocytosed (13). GGT is known to be overexpressed on a variety of cancer cells including ovarian, lung, and prostate cancers (14).

Traditional tumor-targeting therapies have been thought to kill tumor cells selectively. However, even in the same tumor tissues, there exist heterogeneity of receptor densities due to the loss of monoclonality upon proliferation (15). Moreover, the tumor microenvironments have been known to affect tumor cells to change their gene expression patterns (16). Thus, the heterogeneity of tumors caused by the genetic clonal differences or environmental conditions pose major challenges to the success of receptor-specific targeting strategies of nanomaterials (17).

To overcome the heterogeneity of tumor cells per se, there have been approaches to exploit the features of tumor microenvironment such as lower pH (18) or hypoxia (19). We previously reported that anticancer chemotherapy can be selectively activated in tumor microenvironment via cleavage of promellitin to mellitin by fibroblast-activation protein on cancer-associated fibroblasts (20). Although these strategies made substantial progresses in detouring the heterogeneity of target receptor overexpression on tumor cells, there remain

limitations that these strategies cannot modulate the tumor microenvironment, but depend on the physiological feature of tumor microenvironment. However, GGT is one example of tumor receptors known to be affected by tumor microenvironment. Although GGT was not widely studied as a tumor target receptor, GGT has been reported to increase on tumor membranes by the levels of reactive oxygen species (ROS) in the tumor microenvironment (21).

In this study, we hypothesized that the active alteration of tumor microenvironment can reprogram tumor cells to overexpress the target receptors for selective delivery of nanomaterials. To test the hypothesis, we used GGT as a model target receptor, and modulated the ROS in tumor microenvironment by local pretreatment of ROS-generating molecule, methylene blue. For GGT-specific delivery, we designed a hybrid nanoparticle composed of γ-PGA and gold nanoclusters (AuNCs). Here, we report that the microenvironment-controlled tumor cell reprogramming to overexpress GGT could increase the tumor-selective delivery of the hybrid nanoparticles. Moreover, due to the photoresponsiveness of AuNCs, we could selectively kill tumor cells by near infrared light irradiation.

2. Materials and methods

2.1. Preparation of gold and γ-PGA hybrid nanoparticles

Gold and γ-PGA hybrid nanoparticles (Au/PGA hNPs) were prepared by reducing gold ion in the presence of γ-PGA. The aqueous solution of γ-PGA (0.3 mg/mL, Mw, 50 kDa; Bioleaders Corp., Daejeon, Republic of Korea) was added with 2.5 mM of $HAuCl_4 \cdot 3H_2O$ (Sigma-Aldrich, St. Louis, MO, USA) and 0.5 mM of dimethylamine borane (DMAB; Sigma-Aldrich). In some experiments, the concentrations of γ-PGA were varied to prepare Au/PGA hNPs. After vigorous mixing, the reactants were centrifuged at 12,000 g for 5 min. Resulting pellets of Au/PGA hNP were resuspended in 5% of isotonic glucose solution.

2.2. Characterization studies

For the characterization of Au/PGA hNPs, morphology, size, and absorbance spectra were studied. The morphology of Au/PGA hNPs was observed by transmission electron microscopy (TEM). The samples were dried on Formvar/Carbon-coated copper TEM grids (TED Pella, Redding, CA, USA), and observed using TEM (Talos L120C, FEI Company, Hillsboro, OR, USA). The size of Au/PGA hNPs was determined by dynamic light scattering (DLS). For DLS, Au/PGA hNPs were

diluted in TDW then measured using an ELSZ-1000 system (Otsuka Electronics Co. Ltd., Osaka, Japan). UV/Vis absorbance spectra of Au/PGA hNPs were measured in the wavelength of 400-850 nm using a SpectraMAX M5 Microplate Reader (Molecular Devices, San Jose, CA, USA).

2.3. Measurement of photothermal effects

Photothermal effects were examined after irradiation of samples with near infrared light (NIR). The suspensions of the nanoparticles were irradiated for 3 min with 808 nm Fiber DPSS Laser (PSU-FC; ChangChun New Industries Optoelectronics Tech Co. Ltd., Changchun, China) with an output power of 1.5 W. Temperatures of the samples were recorded using an infrared (IR) thermal imaging system (FLIR T420; FLIR Systems Inc., Danderyd, Sweden).

2.4. Cellular induction method of gamma glutamyl transferase

For cellular induction of GGT, MB was used. MCF-7 cells and HeLa cells were cultured in DMEM medium (Welgene, Daegu, Republic of Korea) and RPMI medium (Welgene), respectively. Each medium was supplemented with 10 % of fetal bovine serum, 100 units/mL of penicillin, and 100 μg/mL of streptomycin. The cells were seeded on a 24-well plate. After an overnight

incubation, the HeLa cells were treated with 10 μM of MB (Sigma-Aldrich) solution. After 30 min of incubation, the culture medium was replaced and the MB-treated HeLa cells (HeLa_MB cells) were further incubated overnight.

2.5. Immunostaining of GGT

The induction of GGT on cell membrane was tested by staining with anti-GGT antibodies. MCF-7 cells, HeLa cells, or HeLa_MB cells (1×10^6) were first blocked by incubating for 1 h with 1% bovine serum albumin in phosphate-buffered saline (PBS). The cells were then stained with an anti-GGT1 primary antibody (ab55138, lot #: GR318543-2, Abcam, Cambridge, UK) for 1 h at 1:50 dilution. Next, the cells were stained with a fluorescein isothiocyanate (FITC)-conjugated anti-IgG secondary antibody (sc-2010, lot #: D1315, Santa Cruz Biotechnology, Santa Cruz, CA, USA) for 1 h at 1:50 dilution. The cellular intensity of FITC fluorescence was measured using a BD FACS Calibur equipped with Cell Quest Pro software (BD Bioscience, Franklin Lakes, NJ, USA).

2.6. Cellular uptake assessment

Cellular uptake of the nanoparticles was assessed by measuring the amount of gold. After pretreatment of the cells with or without MB, the cells were incubated for 30 min with 0.5 mg/mL of Au/PGA hNPs, and washed with PBS three times. The

amounts of gold associated with the cells were quantified using an inductively coupled plasma mass spectrometer (ICP-MS; Varian 820-MS, Varian, Sydney, Australia).

2.7. In vitro test of photothermal anticancer effect

MCF-7 cells, HeLa cells, or HeLa_MB cells were treated for 30 min with 0.5 mg/mL of Au/PGA hNPs. The cells were then irradiated for 5 min under 808 nm NIR (ChangChun New Industries Optoelectronics Tech Co. Ltd.) with an output power of 1.5 W. The changes of temperatures were recorded by IR thermal imaging system (FLIR T420). The viability of the NIR-irradiated cells was measured using a 3-(4, 5-dimethylthiazol-2-yl)-2, 5 diphenyltetrazolium bromide (MTT, Sigma-Aldrich) or a fluorescence live-cell staining assay. For MTT assay, the cells were seeded on a 96-well cell plate, incubated overnight, and treated for 2 hr with 0.25 mg/mL of MTT. The cells were treated with 0.1 mL of dimethyl sulfoxide (Junsei Chemical Co. Ltd., Tokyo, Japan), and the absorbance was assessed at 570 nm using a microplate reader (Sunrise Basic; Tecan Group Ltd., Männedorf, Switzerland). Cell viability was expressed as a percentage of that measured in control groups. For the fluorescence live-cell staining assay, the cells were treated with 2 μM of calcein-AM (Biomax, Seoul, Republic of Korea) and observed under a fluorescence microscope (Leica DM, Buffalo Grove, IL, USA).

2.8. In vivo measurement of anticancer effects

In vivo anticancer effects were measured using a tumor xenografted mouse model. Five-week-old female Balb/c athymic nude mice (Raon Bio, Gyeonggi-do, Republic of Korea; approved animal experimental protocol number, SNU-180508-1) were provided with food and water *ad libitum*. The animals were inoculated with 1×10^7 HeLa cells on the right posterior dorsal side. When the tumor volumes reached 50 mm^3, 8 μg/kg of MB dissolved in 5% of isotonic glucose solution was injected locally to HeLa tumor tissues. After 24 hr, mice in each group were intravenously administered with nanoparticles. 24 hr post-dose of nanoparticles, mice were irradiated for 5 min with 808 nm of NIR at an output power of 1.5 W. Temperatures and IR thermal images during the irradiation were recorded using the IR thermal imaging system (FLIR T420). Tumor volumes were calculated by the formula $V = (W^2 \times L)/2$, where V is tumor volume, W is tumor width, and L is tumor length.

2.9. Statistical analysis

Experimental data were statistically evaluated by a two-tailed, one-way analysis of variance (ANOVA) with the Student-Newman-Keuls test as a post hoc test. All statistical analyses were performed using the SigmaStat software (version 3.5; Systat Software, Richmond, CA, USA). A p-value < 0.05 was considered statistically significant.

3. Results

3.1. Characterization of Au/PGA hNPs

As illustrated in Fig. 1, AuNCs were assembled on account of γ-PGA to form Au/PGA hNPs. To find the optimal ratio of γ-PGA monomer of Au/PGA hNPs, glutamic acid residue, and gold in Au/PGA hNPs, physicochemical features of the nanoparticles in five different ratios were characterized. As the molar ratio of γ-PGA monomer and gold changed from 20 : 1 to 1 : 1, color of the nanoparticle suspensions became darker (Fig. 2A). UV/Vis absorbance spectra revealed that the nanoparticle with 1 : 1 molar ratio showed the highest optical density among all five nanoparticles at the range of 400-900 nm wavelength (Fig. 2B).

Hydrodynamic size of the nanoparticle with 1 : 1 molar ratio measured by dynamic light scattering was 125.7 ± 36.4 nm (Fig. 2M). Hydrodynamic size of the other Au/PGA hNPs were getting smaller as a proportion of γ-PGA increased (Fig. 2I-2L). Size of the nanoparticles measured by TEM imaging (Fig. 2C-2H) were consistent with the hydrodynamic size of them (Fig. 2I-2M). Morphology of the 1 : 1, 2 : 1, 3 : 1 samples were round-shaped and were composed of numerous AuNCs (Fig. 2E-2H). On the other hand, at the 10 : 1 and 20 : 1 samples, AuNCs were scattered rather than assembled to become larger nanoparticles (Fig. 2C, 2D).

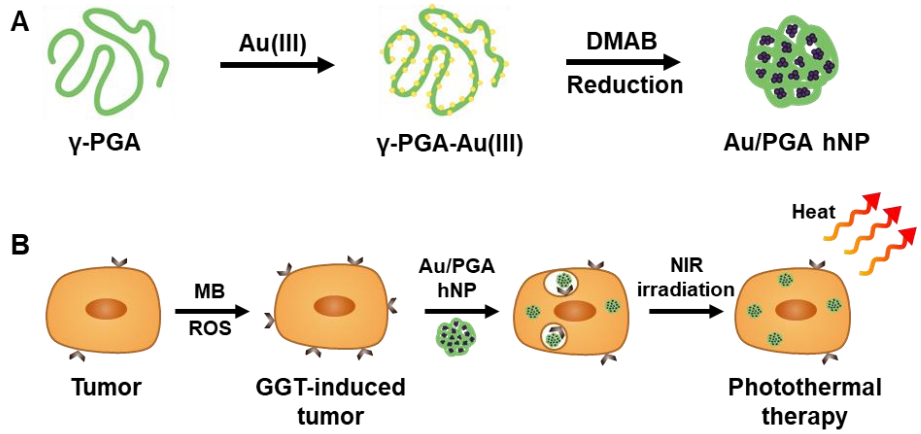

Figure 1. Scheme of the study. A schematic illustration of preparation of Au/PGA hNPs (A), and GGT induction then photothermal therapy using Au/PGA hNPs to tumor cells (B).

Moreover, a temperature of the nanoparticle with 1 : 1 molar ratio increased up to 69.5 ± 0.8 ℃ after 3 min of NIR irradiation (Fig. 2N, 2O). Therefore the 1 : 1 molar ratio was determined to the final formulation and Au/PGA hNP with 1 : 1 molar ratio used in all of the subsequent experiments.

3.2. GGT expression and induction of tumor cells

The pretreatment of HeLa cells with MB induced the expression of GGT on the cell membranes. FACS analysis using a fluorescent anti-GGT1 antibody revealed that HeLa_MB cells had the highest expression of GGT, followed by HeLa and MCF-7 (Fig. 3A). In addition to the induction of GGT, the pretreatment of cells with MB provided the greater increase of Au/PGA hNP. After treatment of Au/PGA hNPs to the cells for 30 min, HeLa_MB cells had the highest cellular uptake, which was identified visually (Fig. 3B) and quantitatively (Fig. 3C). Cellular imaging using TEM (Fig. 3D) revealed that Au/PGA hNPs were bound on the surface of the cells after 30 min of the treatment. Still, HeLa_MB showed the highest cell surface binding of Au/PGA hNPs, compared to the other groups.

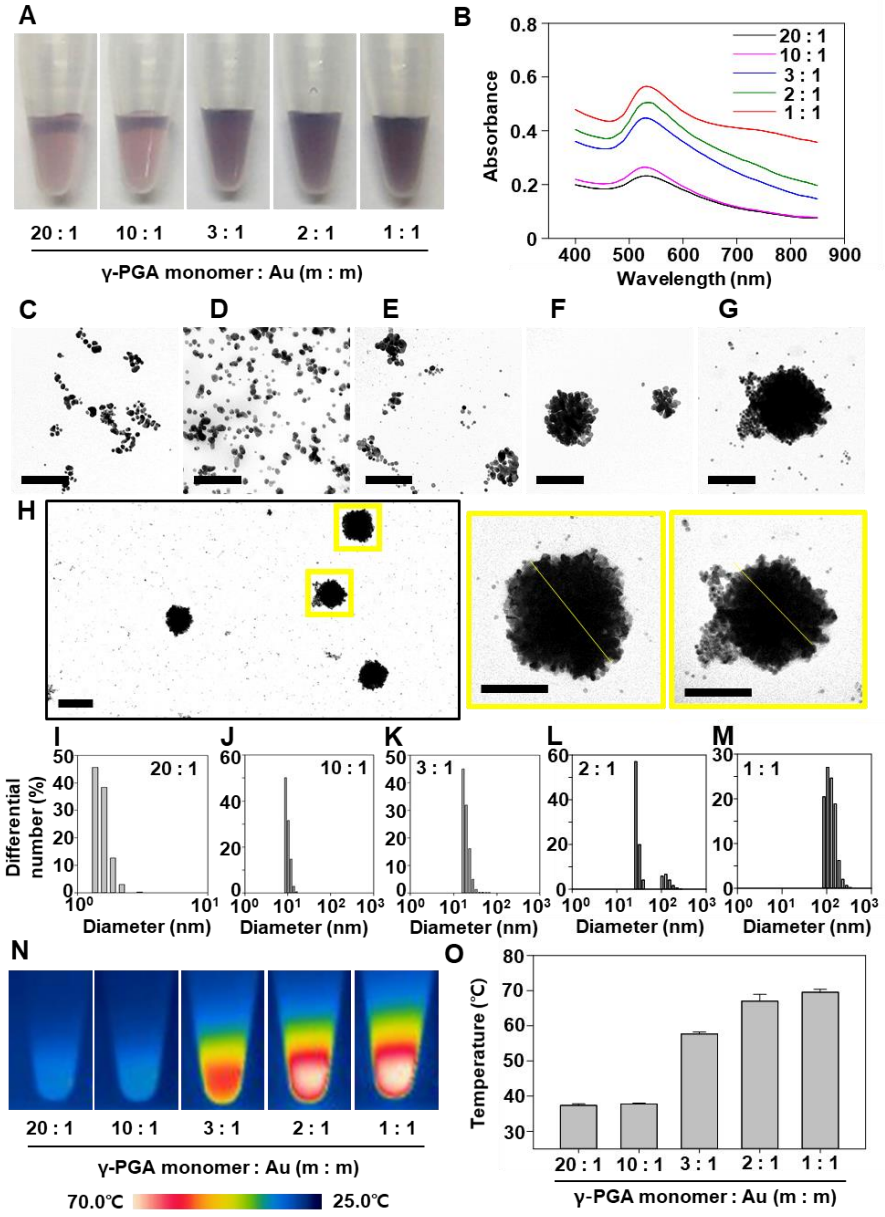
A
20 : 1
10 : 1
3 : 1
2 : 1
1 : 1
γ-PGA monomer : Au (m : m)
B
Absorbance
Wavelength (nm)
C
D
E
F
G
H
I
J
K
L
M
Differential number (%)
Diameter (nm)
N
70.0℃
25.0℃
O
Temperature (℃)

Figure 2. Physicochemical and photothermal properties of Au/PGA hNPs. (A) Photograph of colloidal suspensions of Au/PGA hNPs which molar ratio of glutamic acid residues to gold ions is 20 : 1 to 1 : 1 (left to right). (B) UV/vis absorbance spectra of Au/PGA hNPs. Hydrodynamic size distribution ((C) to (H)) and TEM images ((I) to (M)) of Au/PGA hNPs which molar ratio of glutamic acid residues to gold ions is 20 : 1 ((C) and (I)), 10 : 1 ((D) and (J)), 3 : 1 ((E) and (K)), 2 : 1 ((F) and (L)), and 1 : 1 ((G), (H), and (M)). Scale bars in (C) to (G) represent 100 μm and scale bar in (H) represents 200 μm. Yellow straight lines at (H) represent diameter of Au/PGA hNPs with 1 : 1 molar ratio, which are 192.77 nm (left) and 168.67 nm (right) respectively. Photothermal efficacies of Au/PGA hNPs (N) were measured using a real-time IR thermal camera. (O) Quantitative analysis of images in N.

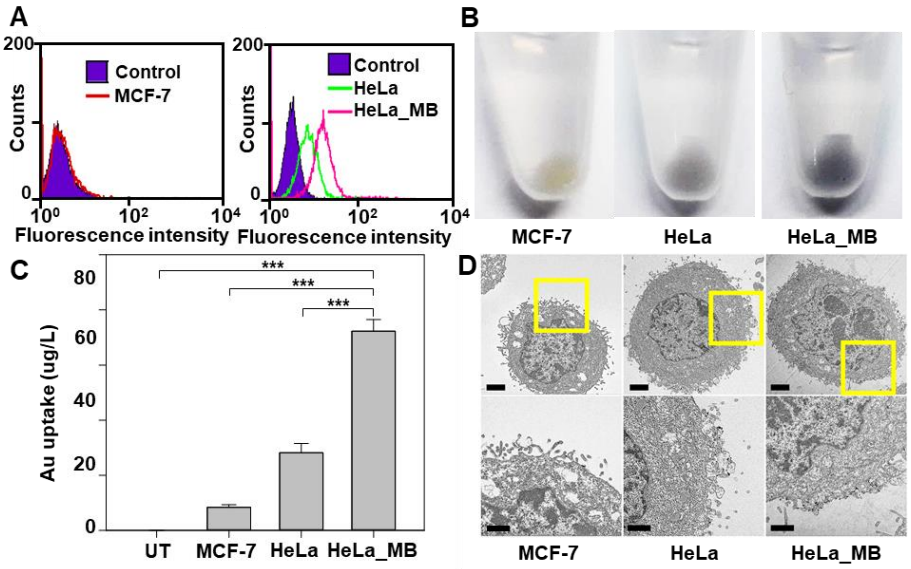

Figure 3. Induction of GGT. GGT expression level of MCF-7, HeLa, and HeLa_MB were assessed using flow cytometry (A) and cellular uptake test of Au/PGA hNPs (B). Results of B were quantitatively analyzed using ICP-MS (C). (D) TEM imaging of Au/PGA hNP-treated cells. Scale bars in the figures on the upper side and the lower side represent 2 μm and 1 μm, respectively. ***$p < 0.005$.

3.3. In vitro control of photothermal anticancer effect by induction of GGT

Photothermal effects of Au/PGA hNPs in vitro were assessed in vitro in MCF−7, HeLa, and HeLa_MB cells. After 5 min of the irradiation, thermal images showed that temperatures of MCF−7 cells increased from 28.6 ± 0.1 ℃ to 33.9 ± 0.5 ℃. In contrast, temperatures of HeLa and HeLa_MB cells increased to 43.9 ± 1.9 ℃ and 50.4 ± 2.1 ℃, respectively (Fig. 4A, 4B). Efficacies of the photothermal therapy were linked to efficacies of killing tumor. Viability of MCF−7 cells was over than 90 % regardless of NIR irradiation. On the other hand, HeLa and HeLa_MB cells on which Au/PGA hNPs were treated then NIR was irradiated respectively showed 62.9 ± 1.7 % and 23.3 ± 4.9 % of viability compared to the cells of same conditions expect NIR irradiation. (Fig. 4C). Similarly, live cell populations were decreased in the order of HeLa_MB, HeLa, MCF−7 cells (Fig. 4D).

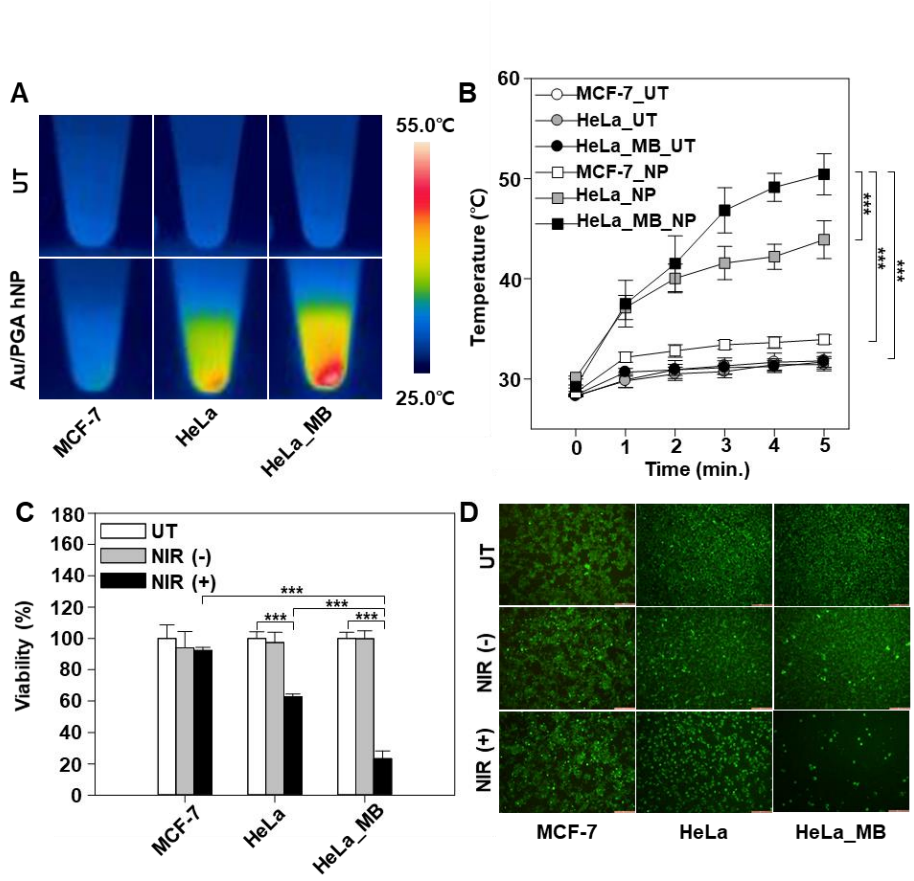

Figure 4. Photothermal antitumor effect of Au/PGA hNPs on GGT-induced cell. MCF-7, HeLa, and HeLa_MB cells were treated with Au/PGA hNPs for 30 min, then irradiated with a NIR laser. Temperatures of the cells following 5 min NIR irradiation (A) were recorded to IR thermal images. Thermal changes of each group (B) were presented. After the irradiation, cells were incubated for 24 hours then viabilities were assessed by MTT assay (C) and live staining (D). ***$p < 0.005$.

3.4. In vivo photothermal and anticancer effects in GGT-induced tumor-bearing mice

Pretreatment of xenografted mice with MB modulated the photothermal anticancer effect of Au/PGA hNP. Au/PGA hNP showed the difference in photoresponsiveness depending on the pretreatment with MB in mice bearing HeLa cell tumors. In the mice untreated with MB, the increase of temperature of tumor tissues after NIR irradiation was 44.9 ± 1.5 ℃ (Fig. 5A, 5B). In contrast, the tumor tissues of mice pretreated with MB, and treated with Au/PGA hNP showed the significant increase of temperature, 59.3 ± 11.8 ℃, upon 808 nm NIR irradiation. Photoablation of tumors was observed in the mice pretreated with MB and treated with Au/PGA hNP, but not in other groups (Fig. 5C, 5D).

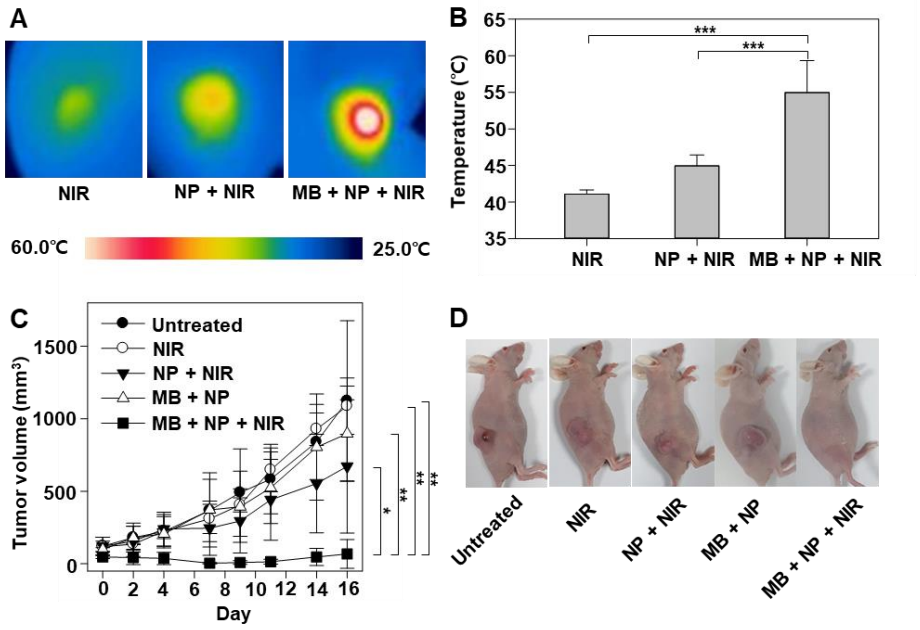

Figure 5. Photothermal antitumor effect of Au/PGA hNPs on GGT-induced tumor bearing mouse. Mice bearing HeLa tumor tissues were administered MB intratumorally, and then injected Au/PGA hNPs intravenously. After 24 h, the tumor sites were irradiated with the NIR laser. (A) Representative images of the tumor sites following 5 min NIR irradiation recorded by the IR thermal camera. (B) Quantitative analysis of images in A. (C) Measurement of tumor growth in mice bearing HeLa tumor tissues, on which NIR was irradiated once 1 day after the inoculation of tumor. (D) Representative images of mice bearing HeLa tumor tissues on day 16. *$p < 0.05$. **$p < 0.01$. ***$p < 0.001$.

4. Discussion

We demonstrated that γ-PGA interacted with gold to form Au/PGA hNPs which were bound to GGT. The pretreatment with MB increased the expression of GGT on tumor cells, and enabled the enhanced delivery of Au/PGA hNP to the tumor cells via GGT.

In this study, Au/PGA hNP was prepared using a facile single step process (Fig 1A). In some studies, gold nanoparticles were prepared first, and additionally conjugated with surface modifying molecules. However, Au/PGA hNP was not the pattern of γ-PGA coating on gold nanoparticles. Rather than specific sizes of gold nanoparticles, AuNCs were formed by reduction of gold ions and mixed with γ-PGA matrix. The sizes of Au/PGA hNP could be controlled by the molar ratios of Au and PGA. We observed that the sizes of Au/PGA hNP tended to decrease with the molar ratios of Au and PGA (Fig. 2C-2M). This tendency has been reported in previous studies (22,23), which used polymers as a matrix of metal nanoclusters. The nanoparticles with lower molar ratio of γ-PGA had relatively larger number of gold ions; so more gold ions would interact with a single γ-PGA polymer. After addition of a reducing agent, γ-PGA would be packed to assemble reduced gold together. γ-PGA interacting with smaller number of gold is hypothesized to be packed less densely, resulting in larger size of Au/PGA hNPs (Fig. 6). Zeta potentials

of Au/PGA hNP increased as the molar ratio of γ-PGA decreased, which supports the hypothesis (data not shown).

The photothermal features of Au/PGA hNP would be attributed to the interparticle plasmon coupling effect of AuNCs dispersed in the γ-PGA matrix of the hybrid nanoparticles. TEM imaging revealed the existence of AuNCs in Au/PGA hNP. Interparticle plasmon coupling effect is known to occur when metal nanoclusters exhibiting SPR are located in proximity (24). These interactions lead the nanoparticles to enhanced photothermal properties. AuNCs in a proximity would cause interparticle plasmon coupling. Au/PGA hNPs of larger size contained larger number of AuNCs (Fig. 2C-2H), which would result in more absorption of UV/Vis light (Fig. 2B) and then result in darker color (Fig. 2A) and higher photothermal efficiency (Fig. 2N, 2O). Therefore Au/PGA hNPs made up of the 1 : 1 molar ratio showed the greatest photothermal therapeutic effect due to the largest number of interparticle coupling between AuNCs.

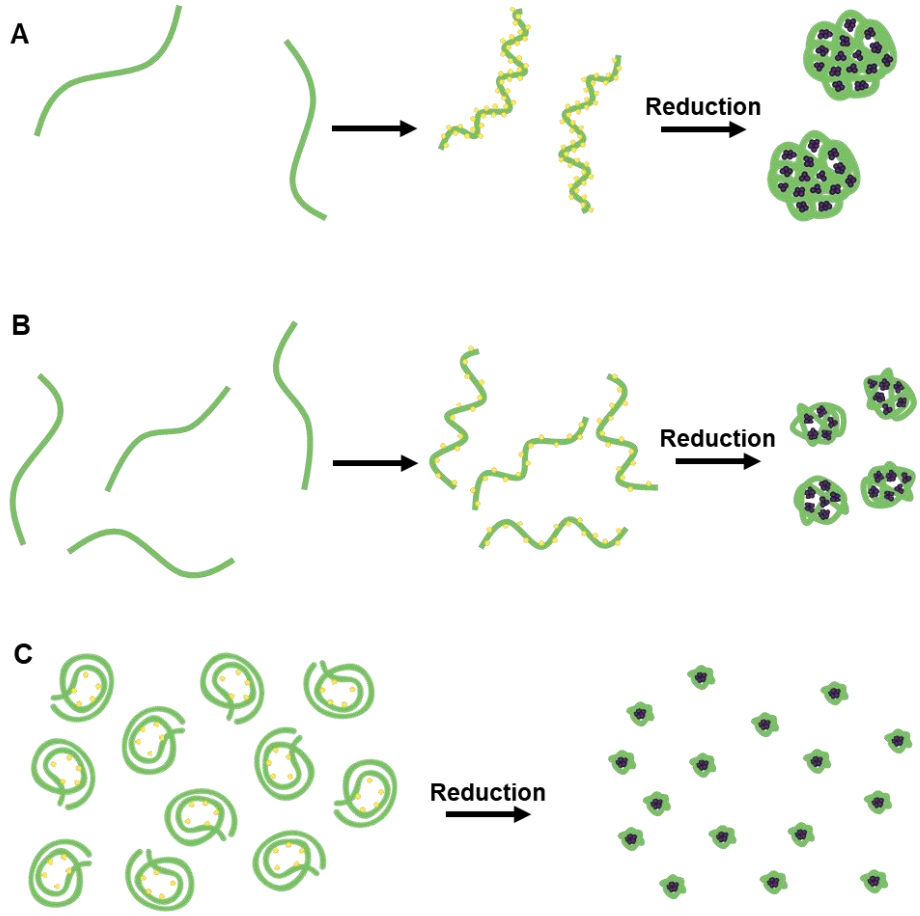

Figure 6. A schematic illustration of the impact of γ-PGA proportion on the size of Au/PGA hNPs. A single γ-PGA polymer interacting with larger number of gold ions (A) and smaller number of gold ions (B) is hypothesized to be packed in a different density after the addition of a reducing agent. The difference in the packing of a polymer would result in difference in size of the nanoparticles. Excess number of γ-PGA polymers compared to gold ions (C) is hypothesized to form Au/PGA hNPs composed of a few number of AuNCs.

There have been few approaches to modulate the expression of target receptors by pretreatment of receptor-inducing agents. The modulation of target receptor expression may have a clear advantage of increasing the efficiency of the induced receptor-mediated delivery of nanoparticles. In addition, the modulated induction of target receptor expression may overcome the heterogeneity of target receptor expression levels among the cells in the tumor tissues. In the case of GGT, although its expression levels on tumor cells are generally upregulated (14), the expression levels are known to be heterogenous among tumor cells according to the genetic, epigenetic factors, and tumor microenvironment (25). The controlling of GGT expression by MB pretreatment may serve as one of effective approaches to overcome the heterogeneity of tumor cells in the tumor tissues.

The mechanism by which the pretreatment with MB induced the expression of GGT is considered to be due to the generation of ROS. In biological microenvironment, MB has been reported to be reduced to leucomethylene blue and generate ROS via NAD(P)H reductase (26). Moreover, GGT is reported to be involved in a glutathione salvage pathway, which increases an intracellular level of glutathione, a major antioxidant acting as a ROS scavenger (Priolo et al., 2018). Although the exact cellular mechanism between ROS and GGT is not known, there is a

rationale that ROS would induce the expression of GGT as GGT contributes to protect cells against oxidative stress.

The enhanced tumor delivery of Au/PGA hNP is attributed to the interaction between γ-PGA and GGT. γ-PGA has been reported to serve as a specific ligand of GGT (13,28). Although in this study we demonstrated the enhanced photothermal efficacy of Au/PGA hNP by induction of GGT, the Au/PGA hNP may be further used for co-delivering chemical drugs to the tumor tissues. Alternatively, exploiting the specific binding of γ-PGA with GGT, amphiphilic derivative of γ-PGA-based nanoparticles may be studied further for induced GGT-mediated delivery of therapeutic cargoes. Previously, we used the amphiphilic derivative of γ-PGA-based nanoparticles for delivery of hydrophobic anticancer drugs (29).

In conclusion, this study showed the potential of modulating the target receptor levels for enhanced delivery of nanoparticles to the tumor tissues. The pretreatment with MB reshaped the tumor microenvironment by boosting the ROS, and sequentially inducing GGT on tumor cell membranes. Due to the specific binding between GGT and γ-PGA, greater tumor delivery and photothermal anticancer efficacy were achieved in Au/PGA hNP-treated group upon MB pretreatment and NIR irradiation. The positively controlled delivery of Au/PGA hNP by modulation of target receptors on tumor cells can serve as an effective strategy to enhance the delivery efficiency as well as

to overcome the heterogeneity of target receptor expression levels among tumor cells. Moreover, the strategy of GGT induction can be further developed to actively modulate the tumor microenvironment for efficacy of targeted delivery of various therapeutic cargoes.

References

(1) Zou L, Wang H, He B, Zeng L, Tan T, Cao H, He X, Zhang Z, Guo S, Li Y. Current approaches of photothermal therapy in treating cancer metastasis with nanotherapeutics. Theranostics. 2016; 6:762-772.

(2) Jung HS, Verwilst P, Sharma A, Shin J, Sessler JL, Kim JS. Organic molecule-based photothermal agents: an expanding photothermal therapy universe. Chem. Soc. Rev. 2018; 47:2280-2297.

(3) Bao Z, Liu X, Liu Y, Liu H, Zhao K. Near-infrared light-responsive inorganic nanomaterials for photothermal therapy. Asian J. Pharm. 2016; 11:349-364.

(4) Lim WQ, Gao Z. Plasmonic nanoparticles in biomedicine. Nano Today. 2016; 11:168-188.

(5) Abadeer NS, Murphy CJ. Recent progress in cancer thermal therapy using gold nanoparticles. J. Phys. Chem. C. 2016; 120:4691-4716.

(6) Amendola V, Pilot R, Frasconi M, Marago OM, Iati MA. Surface plasmon resonance in gold nanoparticles: a review. J. Phys.: Condens. Matter. 2017; 29:203002.

(7) Christau S, Moeller T, Genzer J, Koehler R, von Klitzing R. Salt-induced aggregation of negatively charged gold nanoparticles confined in a polymer brush matrix. Macromolecules. 2017; 50:7333-7343.

(8) Riley RS, Day ES. Gold nanoparticle-mediated photothermal therapy: applications and opportunities for multimodal cancer treatment. Wiley Interdiscip. Rev. Nanomed. Nanobiotechnol. 2017; 9:e1449.

(9) García-Fernández L, Garcia-Pardo J, Tort O, Prior I, Brust M, Casals E, Lorenzo J, Puntes VF. Conserved effects and altered trafficking of cetuximab antibodies conjugated to gold

nanoparticles with precise control of their number and orientation. Nanoscale. 2017; 9:6111-6121.

(10) Wang J, Lu Z, Tang H, Wu L, Wang Z, Wu M, Yi X, Wang J. Multiplexed electrochemical detection of miRNAs from sera of glioma patients at different stages via the novel conjugates of conducting magnetic microbeads and diblock oligonucleotide-modified gold nanoparticles. Anal. Chem. 2017; 89:10834-10840.

(11) Luo S, Tan X, Fang S, Wang Y, Liu T, Wang X, Yuan Y, Sun H, Qi Q, Shi C. Mitochondria-targeted small-molecule fluorophores for dual modal cancer phototherapy. Adv. Funct. Mater. 2016; 26:2826-2835.

(12) Cao M, Feng J, Sirisansaneeyakul S, Song C, Chisti Y. Genetic and metabolic engineering for microbial production of poly-γ-glutamic acid. Biotechnol. Adv. 2018; 36:1424-1433.

(13) Xu F, Zhong H, Chang Y, Li D, Jin H, Zhang M, Wang H, Jiang C, Shen Y, Huang Y. Targeting death receptors for drug-resistant cancer therapy: codelivery of pTRAIL and monensin using dual-targeting and stimuli-responsive self-assembling nanocomposites. Biomaterials. 2018; 158:56-73.

(14) Chiba M, Ichikawa Y, Kamiya M, Komatsu T, Ueno T, Hanaoka K, Nagano T, Lange N, Urano Y. An activatable photosensitizer targeted to γ-glutamyltranspeptidase. Angew. Chem. 2017; 129:10554-10558.

(15) McGranahan N, Swanton C. Clonal heterogeneity and tumor evolution: past, present, and the future. Cell. 2017; 168:613-628.

(16) Zhang C, Guan Y, Sun Y, Ai D, Guo Q. Tumor heterogeneity and circulating tumor cells. Cancer Lett. 2016; 374:216-223.

(17) Chung SW, Choi JU, Cho YS, Kim HR, Won TH, Dimitrion P, Jeon OC, Kim SW, Kim IS, Kim SY, Byun Y. Self-triggered apoptosis enzyme prodrug therapy (STAEPT): enhancing

targeted therapies via recurrent bystander killing effect by exploiting caspase-cleavable linker. Adv. Sci. 2018; 5:1800368.

(18) Guo X, Wang L, Duval K, Fan J, Zhou S, Chen Z. Dimeric drug polymeric micelles with acid-active tumor targeting and FRET-traceable drug release. Adv. Mater. 2018; 30:1705436.

(19) Huo D, Liu S, Zhang C, He J, Zhou Z, Zhang H, Hu Y. Hypoxia-targeting, tumor microenvironment responsive nanocluster bomb for radical-enhanced radiotherapy. ACS Nano. 2017; 11:10159-10174.

(20) Kim MG, Shon Y, Kim J, Oh YK. Selective activation of anticancer chemotherapy by cancer-associated fibroblasts in the tumor microenvironment. J. Natl. Cancer Inst. 2017; 109:djw186.

(21) Hanigan MH. Gamma-glutamyl transpeptidase: redox regulation and drug resistance. In Adv. Cancer Res. 2014; 122:103-141. Academic Press.

(22) Xie J, Zheng Y, and Ying JY. Protein-directed synthesis of highly fluorescent gold nanoclusters. J. Am. Chem. Soc. 2009; 131:888-889.

(23) Yoon GJ, Lee SY, Lee SB, Park GY, Choi JH. Synthesis of iron oxide/gold composite nanoparticles using polyethyleneimine as a polymeric active stabilizer for development of a dual imaging probe. Nanomaterials. 2018; 8:300.

(24) Song W, Ding L, Chen Y, Ju H. Plasmonic coupling of dual gold nanoprobes for SERS imaging of sialic acids on living cells. Chem. Commun. 2016; 52:10640-10643.

(25) Pitynski K, Ozimek T, Galuszka N, Banas T, Milian-Ciesielska K, Pietrus M, Okon K, Mikos M, Juszczyk G, Sinczak-Kuta A, Stoj A. Association of the immunohistochemical detection of gamma-glutamyl transferase expression with clinicopathological findings in postmenopausal women with endometrioid adenocarcinoma

of the uterus. J. Physiol. Pharmacol. 2016; 67:395-402.

(26) Han L, Chen Y, Niu J, Peng L, Mao Z, Gao C. Encapsulation of a photosensitizer into cell membrane capsules for photodynamic therapy. RSC Adv. 2016; 6:37212-37220.

(27) Priolo C, Khabibullin D, Reznik E, Filippakis H, Ogórek B, Kavanagh TR, Nijmeh J, Herbert ZT, Asara JM, Kwiatkowski DJ, Wu CL. Impairment of gamma-glutamyl transferase 1 activity in the metabolic pathogenesis of chromophobe renal cell carcinoma. Proc. Natl. Acad. Sci. U.S.A. 2018; 115:E6274-E6282.

(28) Tan J, Wang H, Xu F, Chen Y, Zhang M, Peng H, Sun X, Shen Y, Huang Y. Poly-γ-glutamic acid-based GGT-targeting and surface camouflage strategy for improving cervical cancer gene therapy. J. Mater. Chem. B, 2017; 5:1315-1327.

(29) Shim G, Kim D, Kim J, Suh MS, Kim YK, Oh YK. Bacteriomimetic poly-γ-glutamic acid surface coating for hemocompatibility and safety of nanomaterials. Nanotoxicology. 2017; 11:762-770.

국문초록

입자간 플라스몬 나노입자의 특이적 전달을 위한 종양미세환경 조절을 이용한 종양세포 재프로그래밍

이다운

약학과 물리약학전공

서울대학교

본 연구에서는 금 나노클러스터와 폴리감마글루탐산(poly-γ-glutamic acid; PGA)을 이용한 간단하고, 생체적합성이 뛰어나며, 광열 활성을 띠는 나노입자를 형성하였다. 그리고 국소적으로 활성산소종 (reactive oxygen species; ROS)을 유발시켜 암세포 표면의 특정 수용체의 과발현을 유도하여 나노입자의 전달 효율을 높였다. 금 3가 이온에 환원제를 첨가하면 금으로 환원되는데, 이 때 폴리감마글루탐산이 뼈대로 작용하여 직경 10 나노미터 이하의 금 나노클러스터로 구성된 금/PGA 하이브리드 나노입자 (Au/PGA

hNP)를 형성하였다. Au/PGA hNP는 그 안에 함유한 금 나노클러스터의 수가 많을수록 더 큰 광열효과를 나타내었는데, 입자간 플라즈몬 커플링 효과 (interparticle plasmon coupling effect)가 이 현상에 기인하는 것으로 추정된다. 한편, PGA는 암세포 표면에 발현하는 수용체인 감마 글루타밀 전이효소 (gamma glutamyl transferase; GGT)의 리간드로 작용할 수 있다는 것이 알려져 있다. 세포 실험에서 메틸렌 블루의 투여를 통해 발생한 ROS는 GGT의 과발현을 유도하여 Au/PGA hNP의 세포 내로의 섭취 증가를 일으켰다. 808 nm 근적외선 레이저를 조사하였을 때, GGT가 유도된 HeLa 세포의 온도는 다른 그룹에 비해 가장 많이 상승하였고 이로 인해 가장 강력한 암세포 사멸 효과를 보였다. 종양이식 마우스에 Au/PGA hNP를 정맥 투여한 후 종양 조직에 808 nm 근적외선 레이저를 조사하였을 때, 마찬가지로 GGT가 유도된 HeLa 세포 조직에서 가장 높은 광열효과와 암세포 사멸 효과를 보였다. 이러한 결과들을 통해, 입자간 플라즈몬 커플링 효과를 일으키는 Au/PGA hNP와, ROS 유발물질의 국소 투여를 통한 GGT 발현 유도는 암세포-표적 광열 치료 효능을 더욱 증대시킨다는 것을 시사한다.

주요어 : 종양세포 재프로그래밍; 종양미세환경; 활성산소종; 종양 이종성; 수용체 매개 전달, 입자간 플라즈몬 커플링

학번 : 2017-21431